Journal: Physical Review E

Accession code: EF12685

Article Title: Subphase with four-layer superlattice structure confirmed by resonant soft x-ray scattering
in thresholdless antiferroelectric liquid crystal mixtures

First Author: Yoichi Takanishi

AUTHOR QUERIES - TO BE ANSWERED BY THE CORRESPONDING AUTHOR

The following queries have arisen during the typesetting of your manuscript. Please answer these queries by marking the required corrections at the appropriate point in the text.

1	Please verify affiliation #1.
2	Please check the Data Availability statement. Is Ref. [1] as meant here?
3	Please verify updated Ref. [10].
4	Please note that duplicate reference were detected (i.e., Refs. [10] and [11]) and provide instructions for which should be deleted or amended. We can perform renumbering of references if you provide simple instructions.
5	Ref. [20,21]: Please double-check all information and provide journal/publisher name, volume, page no., and valid doi/url, if available.
6	Please provide publisher name and location for all book references.
FQ	This funding provider could not be uniquely identified during our search of the FundRef registry (or no Contract or Grant number was detected). Please check information and amend if incomplete or incorrect.

Ans. 1; Atsuo Fukuda: 0000-0001-7119-3645, Hiroshi Iwayama: 0000-0002-5992-5281, Neelam Yadav: 0000-0001-8046-3280

Ans. 2; Please change to "Data can be obtained from the contact authors by making reasonable request."

Ans. 3; No, please change it back to the previous one.

Ans. 4; By addressing the Queriy 3, it will no longer be a duplicate.

Ans. 5; We changed the references the same as Shirota et al., PRE 107, 064701 (2023).

Ans. 6; We changed the references the same as Shirota et al., PRE 107, 064701 (2023).

Important Notice to Authors

Attached is a PDF proof of your forthcoming article in PRE. Your article has 14 pages and the Accession Code is **EF12685**.

Your paper will be in the following section of the journal: REGULAR ARTICLES

No further publication processing will occur until we receive your response to this proof.

All articles are converted to standardized XML, which generates the PDF and online versions and populates third-party systems (e.g., Portico, Crossref, Web of Science). This process works well for most articles, but please carefully check all key elements in your PDF proof, especially equations and tables.

ORCIDs https://orcid.org/

- Follow any ORCID links () after the authors' names and verify that they point to the appropriate record.
- Requests to add ORCIDs should be sent only during the first proof revisions (not before or after). If authors do not subsequently add/authenticate ORCIDs within seven business days, production of the paper will proceed and no further requests to add ORCIDs will be processed. See complete details regarding ORCID requests and ORCID verification at https://journals.aps.org/authors/adding-orcids-during-proof-corrections.
- If this paper is an Erratum or a Reply, the corresponding author's ORCID may be present if previously provided to APS, but no ORCIDs can be added at proof stage.

Research Organization Registry ID (ROR) https://ror.org/

- Ensure affiliations have been correctly identified by clicking on any institution names that have been linked to the ROR database (blue text). Note that affiliations will be linked to their parent institution's ROR ID (if available) if they do not have a separate ID. If no appropriate ID is available, there will be no link. Links cannot be removed for correctly linked affiliations.
- Information about an author's research organization is submitted to Crossref as part of the metadata for articles published by APS.

Data Availability Statement (DAS) https://journals.aps.org/authors/data-availability-statements

- The DAS you selected when you submitted/resubmitted your manuscript has been added to the proof.
- Please check the statement and add any missing information, e.g., description of data, reference citations.
- Ensure a reference or references giving details of where the data can be accessed is given in the reference list and cited in the DAS. The reference should include the authors (creators) of the data, any version number, the name of the repository (if applicable), the year the data was published, and a persistent identifier. Follow linked DOIs/URLs to ensure they link to the data.

Crossref Funder Registry ID https://www.crossref.org/services/funder-registry/

- Ensure acknowledgments include all sources of funding for your article, following any requirements of your funding sources. Where possible, please include grant and award ids.
- Information about an article's funding sources is submitted to Crossref to help you comply with funding agency mandates. Crossref's Funder Registry is the definitive registry of funding agencies.

Please carefully check the following funder information we have already extracted from your article and ensure its accuracy and completeness:

- MGC, MC881, MC815, MC452
- US-Ireland collaborative program, SFI 21/US/3788
- IMS, 23IMS6819, 23IMS6621, 24IMS6616
- Photon Factory Advisory Committee, 2025G118
- JSPS, 21K2523

Overall, please proofread the entire formatted article very carefully. The redlined PDF should be used as a guide to see changes that were made during copyediting. However, note that some changes to math and/or layout may not be indicated.

Other Items to Check

- All key elements of the paper, particularly the equations and tabular data. (The original manuscript has been converted to XML prior to the creation of the PDF proof, as described above.)
- Title: It may have changed during the peer-review process.
- Author list: Ensure all names are spelled correctly and all authors are presented in the appropriate order, especially if you have used the "groupedaddress" option in REVTeX, which is the default setting and will order authors by institution, not in the order the names were entered.
- Contact author: Ensure there is a byline footnote containing an email address for the author(s) wishing to receive correspondence from readers. (Contact author: author@email.com). All emails provided on the paper will be labeled as contact authors. A contact author does not have to be the corresponding author (see https://journals.aps.org/authors/editorial-policies-authorship#responsibilities).
- Affiliations: Affiliation(s) must be where the research was conducted. Ensure institution names are spelled correctly and attributed to the appropriate author(s). Click on any institution names that have been linked to the ROR database (blue text) to ensure they are correctly identified.
- Receipt date: Please confirm accuracy.
- Acknowledgments: Appropriately acknowledge all funding sources.
- Hyphenation: Please note APS style:
  - Hyphens may have been inserted in word pairs that function as adjectives when they occur before a noun, as in "gamma-ray detection," "4-mm-long gas cell," and "R-matrix theory."
  - Hyphens are deleted from word pairs when they are not used as adjectives before nouns, as in "electric fields of gamma rays," "was 4 mm in length," and "the R matrix is tested."
  - Hyphens are not used after prefixes or before suffixes: superresolution, quasiequilibrium, nanoprecipitates, resonancelike, clockwise.
- Figures:
  - Ensure they are accurate and sized properly.
  - Check that all labeling is legible.
  - If you revise any figures, please indicate clearly if any data or results have changed.
  - Figure quality in the proof is representative of the quality to be used in the online journal. Some compression and downsampling of figures may have occurred. Fine details may have become somewhat fuzzy, especially in color figures. The print journal uses higher resolution files and therefore details may be sharper in print.
  - Figures submitted as separate files containing color appear in color on these proofs and in the online journal.
  - For information on color in the print journal see https://journals.aps.org/prl/authors#pubcharges.
- References: Missing article titles have been added. Please check.
- Supplemental material (SM): Files will not be copyedited or altered by APS after submission and should be submitted in a format ready to be published. You will not receive page proofs of SM. If references in the main text are renumbered, SM cites to those references may also need to be renumbered and a revised file submitted. For more information see https://journals.aps.org/authors/supplemental-material-instructions.

Ways to Respond

- Web: If you accessed this proof online, follow the instructions on the web page to submit corrections.
- Email: Send corrections to preproofs@aptaracorp.com

PHYSICAL REVIEW E **00**, 005400 (2026)

Subphase with four-layer superlattice structure confirmed by resonant soft x-ray scattering in thresholdless antiferroelectric liquid crystal mixtures

Yoichi Takanishi,[1,*] Neelam Yadav,[2] Vitaly P. Panov,[2,3] Hiroshi Iwayama,[4] Fumito Araoka,[5] Atsuo Fukuda,[2,†] and Jagdish K. Vij[2,‡]

[1]*Department of Physics, Kyoto Prefectural University of Medicine, Kyoto-shi 602-8566, Japan*

[2]*Department of Electronic and Electrical Engineering, Trinity College Dublin, The University of Dublin, Dublin 2, Ireland*

[3]*School of Electronic and Electrical Engineering, Sungkyunkwan University, Suwon 16419, Gyeonggi Do, South Korea*

[4]*UVSOR Synchrotron Facility, Institute for Molecular Science, Okazaki, Aichi 444-8585, Japan*

[5]*RIKEN Center for Emergent Matter Science, Hirosawa 2-1, Wako, Saitama 351-0198, Japan*

(Received 5 June 2025; revised 30 January 2026; accepted 23 March 2026; published xxxxxxxxxx)

Binary mixtures developed as thresholdless antiferroelectric (TLAF) materials, MC881-MC815 and MC881-MC452, are studied using optical rotatory power (ORP), resonant soft x-ray scattering (RSoXS), and dynamic light scattering (DLS). A single subphase is confirmed to exist in both mixtures by ORP, stably over a wide temperature range (around 80°C below RT) but in a narrow concentration range (1–3 wt.%), with curved boundaries; between SmC_A^* and the subphase, the ratio of synclinic and anticlinic orderings changes continuously. The antiferroelectric four-layer superlattice structure of the subphase is now firmly established by RSoXS using free-standing films, although a two-layer SmC_A^* structure is observed in silicon nitride membrane cells often used in RSoXS, highlighting the influence of surface conditions. The TLAF properties of the subphase are confirmed in homogeneously aligned cells by observing apparent tilt angles induced by an applied electric field. The relaxation times responsible for the TLAF properties are studied by DLS, indicating the smooth flip-flopping of a group of molecules in a single layer, which must also be responsible for the continuous change among SmC_A^*, the subphase, and SmC^*. Each smectic layer appears to play an important role as a *mesoscopic* entity.

DOI: 10.1103/wtm3-czy1

I. INTRODUCTION

The discovery of a ferroelectric liquid crystal and the subsequent development of surface-stabilized ferroelectric liquid crystal displays (FLCDs) opened a new era of FLCDs and related materials [1–3]. Many material and chemical manufacturers showed keen interest in FLCDs, and a large number of chiral smectic liquid crystal compounds were designed and synthesized and their mixtures were developed. Among these, an antiferroelectric liquid crystal was discovered [4]. The polar phenomena in chiral smectic liquid crystals involved the clinicity frustration in antiferroelectric anticlinic SmC_A^*, ferroelectric synclinic SmC^*, and paraelectric orthogonal SmA. The frustration together with the long-range interlayer interactions produces optically uniaxial SmC_α^* and various biaxial subphases in the vicinity of the three basic main phases, SmC_A^*, SmC^*, and SmA. The temperature-induced successive transitions via the main phases and subphases are observed in a variety of pure compounds and their mixtures, and the subphase temperature range is usually as narrow as a few degrees centigrade or less. The phase transitions are of the first order and these are characterized by abrupt changes, except for a continuous change in some cases between SmC^* and SmC_α^*. The biaxial subphases are reasonably designated by the unit cell size and/or the q_T number given by

$$q_T = \frac{[F]}{[A]+[F]}, \tag{1}$$

where $[F]$ and $[A]$ are the numbers of synclinic ferroelectric and anticlinic antiferroelectric orderings, respectively. Among them the ferrielectric subphase with three-layer (FAA) unit cell, SmC_{d3} and/or q_T=1/3, and the antiferroelectric subphase with four-layer ($FAFA$) unit cell, SmC_{d4} and/or q_T=1/2, are frequently observed. The biaxial and optically uniaxial subphases are characterized by commensurate highly distorted and incommensurate neat helical structures, respectively [5].

In review papers published in 2010s [6–8], the direct interactions not only between the nearest-neighbor (adjacent) layers but also between the next-nearest-neighbor layers were considered to play an essential role in the emergence of the biaxial subphases and the nanometer-pitch helical structure of SmC_α^* as well as the anticlinic structure of SmC_A^* itself. In systems like smectic liquid crystals where the positional order is disordered, however, it is difficult to imagine that any proper interaction may be directly operative even between the next-nearest-neighbor layers. In fact, we had insisted on the importance of other mechanisms too. The appearance of the anticlinic structure is due to the orientational correlation of the lateral dipoles between adjacent layers [9,10], and the emergence of the biaxial subphases is caused by the effective long-range interlayer interactions (LRILIs) derived from *the discrete flexoelectirc effect* that also depends only on the interactions between the adjacent layers [11–13]. By

*Contact author: ytakanis@koto.kpu-m.ac.jp
†Contact author: fukudaa@tcd.ie
‡Contact author: jvij@tcd.ie

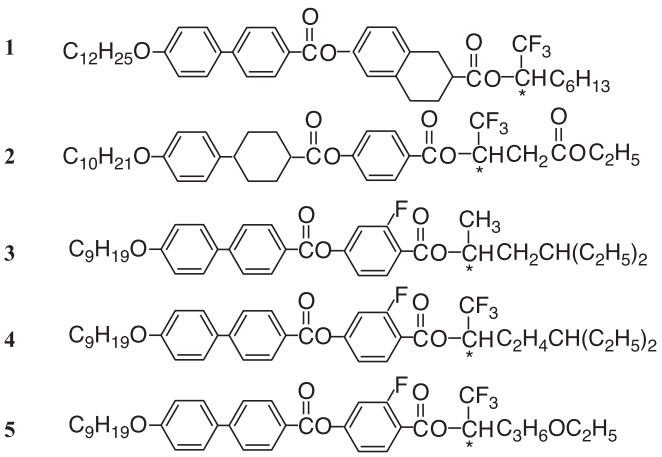

FIG. 1. Chemical structural formulas of TLAF materials. Mitsui Chemicals reported compounds **1** and **2** as Mitsui mixture. Compounds **3**, **4**, and **5** were developed by Mitsubishi Gas Chemical (MGC), the product numbers of which are MC881 (antiferroelectric), MC815 (ferroelectric), and MC452 (ferroelectric), respectively.[1] All the MGC compounds are the (*R*) moieties. See text for details.

combining the phase diagram of SmC_A^*, SmC^*, and SmA with the effective LRILIs, a comprehensive model was constructed so that the emerging sequence of subphases and their intriguing properties can be systematically understood. The importance of the discrete flexoelectric effect is clearly demonstrated by the emergence of $q_T = 1/4, 2/5$, and 1/7 subphases with large unit cells consisting of 8, 10, and 7 smectic layers, respectively, and the electric field-induced transition of SmC_α^* to biaxial ferrielectric and antiferroelectric q_T=1/3 and 1/2 subphases [14–16]. In spite of the overall success in constructing the comprehensive model based on the degeneracy lifting due to the effective LRILIs at the frustration point, there exist some cases where not only the effective LRILIs but the *thermal fluctuations* also play an important role [18,19]. This phenomenon is especially observed in mixtures of the materials developed by two Japanese companies, Mitsui Chemicals and Mitsubishi Gas Chemical (MGC) [20–22], as the thresholdless antiferroelectric (TLAF) materials. The chemical structures of these compounds are shown in Fig. 1. It seems that they prepared binary mixtures of strong antiferroelectric and ferroelectric compounds and obtained the desired properties near the boundary, which becomes parallel to the temperature axis, i.e., vertical to the concentration abscissa axis; this was predictable based on previous systematic experiments on phase diagrams of binary mixtures [23]. Actually, Sandhya *et al.* [24–26] carefully studied MC881-MC452 in the concentration range around the boundary by using Bragg reflection spectra due to the director helical structure. They confirmed the emergence of a single subphase stabilized along the borderline on its low concentration side; its stability temperature range is exceptionally wide from around 80°C down to below zero, but the concentration range of the mixture is as narrow as about 3 wt.%. Furthermore, they noticed that q_T continuously becomes larger with increasing temperature on both concentration sides of the subphase. On the low concentration side, q_T increases from 0 to 1 with increasing temperature, i.e., SmC_A^* gradually changes to SmC^*; on the high concentration side of the subphase, q_T also becomes larger with rising temperature and approaches to 1 but does not seem to start from 0, i.e., SmC^* emerges at high temperatures but SmC_A^* does not seem to exist even at low enough temperatures.

In this paper we study the mixtures developed by MGC, as MGC kindly donated large amounts of key compounds to one of the authors (A.F.) when they unfortunately stopped the R&D of TLAF materials in 2006. Actually, MC881-MC452 studied by Sandhya *et al.* [24–26] was an early developed mixture; MGC insisted that another MC881-MC815 mixture shows much more suitably desirable TLAF properties [27], where the emergence of a single subphase along the border line had not been confirmed as yet. Since it takes a very long time to observe the Bragg reflection spectra systematically, we first show that by measuring the optical rotatory power we can determine the existence of a subphase in MC881-MC452 at finer temperature and concentration intervals; thus we confirm the subphase emergence along the borderline even in MC881-MC815. At the same time, we modify the details of the previously obtained T-r phase diagram of MC881-MC452 [25,26,28]. In Sec. III B, we explain the subphase unit cell structure determined unambiguously by resonant soft x-ray scattering (RSoXS) at the carbon K-edge [29–31], where the sample cell should be thin enough to be properly transparent to the incident beam. Actually, the structure critically depends on the sample surface conditions in prepared thin samples: The subphase shows the two-layer (*AA*) unit cell in samples sandwiched between about 100 nm thick silicon nitride membranes, whereas the four-layer (*FAFA*) unit cell is confirmed in a sample spread over a TEM grid with a spatula. In Sec. III C, we demonstrate the TLAF properties of the subphase in MC881-MC452 and MC881-MC815 by observing the apparent tilt angles induced by an applied electric field in homogeneously aligned cells. And furthermore, although preliminarily in the sense that the concentrations were not previously recorded, the relaxation times responsible for the TLAF properties of MC881 containing 53.7 wt.% MC452 are obtained by measuring the intensity autocorrelation functions in DLS.

II. EXPERIMENTS

The properties of MC881-MC452 and MC881-MC815 are known to change significantly with slight variations in mixing ratios near the critical concentration r_c. We prepared each mixture very carefully so that the concentration reproducibility of better than ±0.005 wt.% is guaranteed, at least relatively, by using a Shimazu microbalance with the accuracy in weight of ±1 μg. Acetone was used to ensure the mixture of compounds became homogeneous and the complete evaporation of the solvent in the mixture was checked by weighing the sample bottle before the addition of acetone and after its evaporation. Experimental details of measuring ORP by using a photoelastic modulator (PEM-90, Hinds Instruments)

[1]MGC considered that these ferroelectric compounds must be ferrielectric because of their characteristic conoscopic behavior. However, Song *et al.* clearly showed that these are ferroelectric [17].

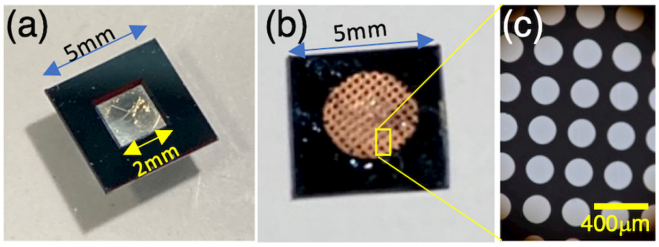

FIG. 2. Photographs of used sample cells for RSoXS: (a) a membrane sandwiched cell, (b) a copper grid for transmission electron microscopy (TEM). (c) Microphotograph of the holes in the copper grid.

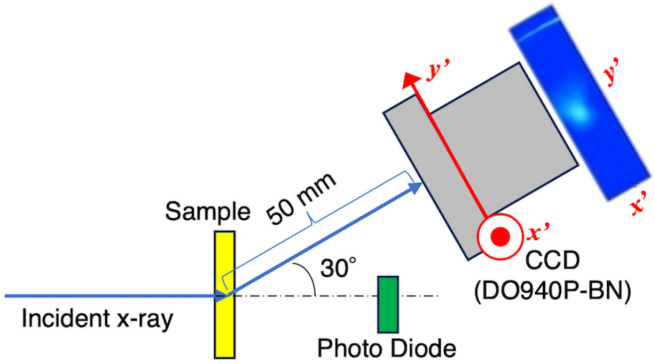

FIG. 3. Geometry for RSoXS and obtained scattering image. x' and y' are horizontal and vertical direction of the surface of the CCD camera, respectively.

were given in previous papers [32–34]. The actual measurements were made mainly in Dublin and supplementally in Kyoto. The light source used was a He-Ne laser (633 nm). Response time of the lock-in amplifier (SR830 DSP, Stanford Research Systems) is 1 s, and data capture time of the computer is 3 s. Temperature changing rate is 1∼5°C/h at a step of 0.01∼0.05°C. Once it is confirmed that the set temperature has been reached, the measured ORP value is recorded in the computer. Homeotropically aligned cells, where the smectic layers are parallel to the substrate surfaces in Sm*A*, were used. (These cells are sometimes called vertical aligned cells, since the constituent rod-like molecules are perpendicular to the substrate surfaces.) Hereafter we simply call them homeotropic cells in this paper. The cell thickness was about 20 μm. We first measured ORP by decreasing the temperature down to 30°C and then observed it by increasing the temperature. For the RSoXS measurements [29–31], two types of homogeneously aligned cells were prepared, where the smectic layers are perpendicular to the substrate surfaces in Sm*A*. (These cells are sometimes called planar aligned cells, since the constituent rod-like molecules are parallel to the substrate surfaces.) Hereafter we simply call them homogeneous cells in this paper. In the soft x-ray wavelength region, silicon nitride membranes are frequently used as substrates; hence the first type was a homogeneous cell sandwiched between 100-nm-thick silicon nitride membranes (NX5200C, Norcada). The membrane is mounted on a 200-μm-thick, 5-mm-square silicon frame as shown in Fig. 2(a).

The sample was injected into the membrane sandwiched cell in the isotropic phase and was cooled to RT at a rate of 6°C/h. The cell gap was kept at about several hundreds of nanometers by checking the color of the optical birefringence. The obtained homogeneous cell was multidomain since no special alignment treatment was applied to the silicon nitride membranes; the domain size was much smaller than the soft x-ray beam spot size (200 μm × 400 μm), and hence the obtained scattering image was powder pattern. To become free from the supposedly strong interface effects of the silicon nitride membranes, we tried a free standing film sample as the second type of homogeneous cell. Since it usually shows homeotropic alignment, a transmission electron microscopy (TEM) grid was used in the hope that homogeneous alignment on the copper grid would prevail over the hole area; liquid crystal sample was coated using a spatula at RT. The actually used TEM grid (Cu 100-A, Oken Shoji) is made of 25-μm-thick copper whose hole size is 200 μmϕ, as shown in Figs. 2(b) and 2(c). Here we call it a TEM grid cell. The thickness of the liquid crystal was somewhat uncertain, but the RSoXS measurements were performed under conditions where the transmittance of the incident x-ray was approximately 30∼50%.

RSoXS measurements were performed at BL3U of UVSOR beam line of Institute for Molecular Science (Okazaki, Aichi). Experimental setup was shown in Fig. 3. The sample cells were mounted in a sample holder and placed in the vacuum chamber; the degree of vacuum around the sample was kept at less than 10^{-2} Pa, whereas the degree of vacuum of x-ray beam incident area was ca. 1×10^{-6} Pa. The temperature of samples was controlled by a hand-made oven with a temperature controller (DB-1230, Chino). The x-ray scattering was detected by a CCD camera (DO940P-BN, Andor), and the camera length was 50 mm. The CCD camera can cover the scattering angle 2θ from 14.6 to 43.5 deg. Incident x-ray energy was tuned from 270 to 290 eV, which can cover the absorption energy of carbon K-edge (ca. 285 eV). Behind the sample, the photodiode for measuring the transmittance of an incident x-ray beam can be inserted and removed as required. Typical absorption spectrum was shown in Fig. 4,

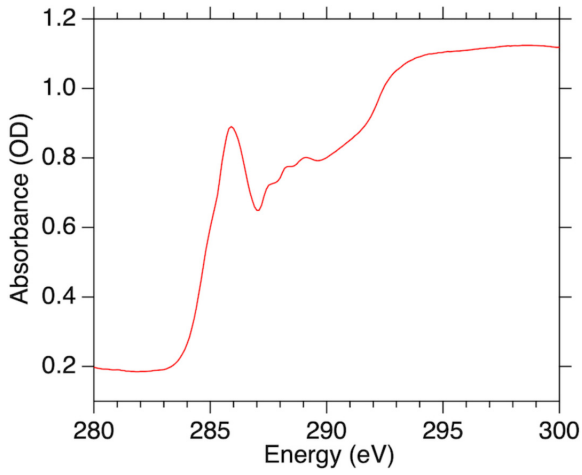

FIG. 4. Absorption spectrum of MC881 containing 55.7 wt.% MC452.

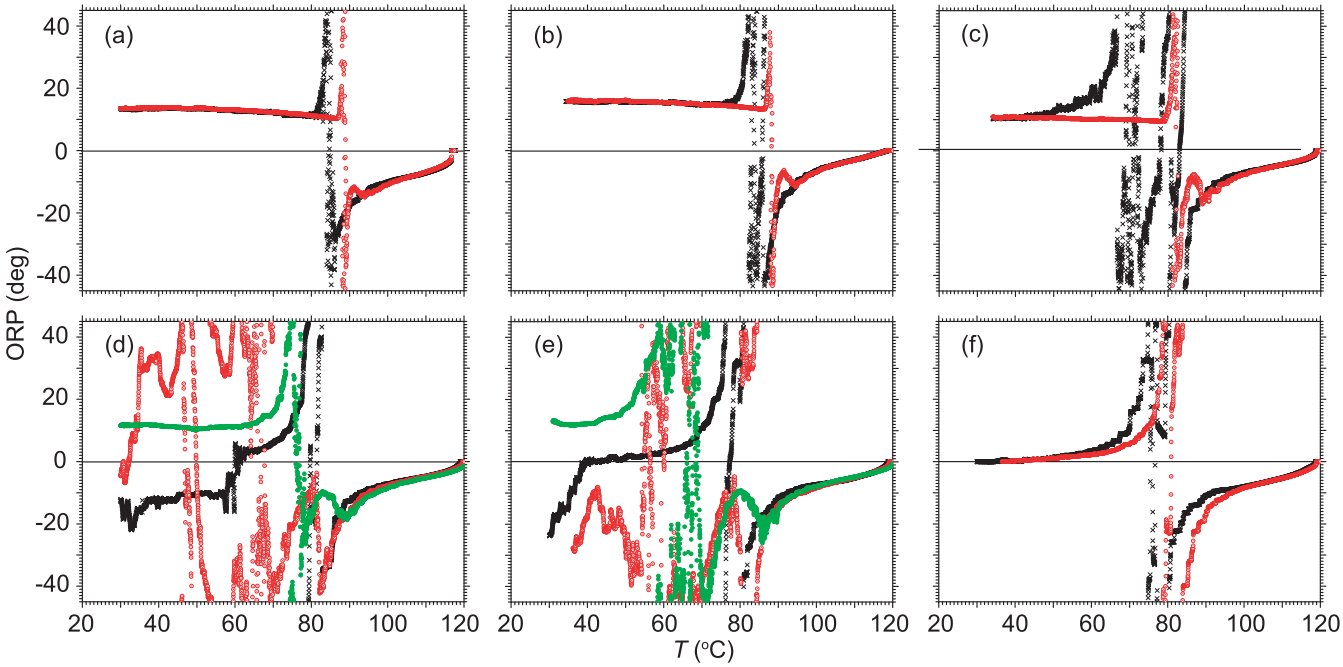

FIG. 5. ORP vs temperature in MC881 containing MC452 of (a) 56.00, (b) 57.00, (c) 57.98, (d) 58.50, (e) 59.00, and (f) 60.01 wt.%; red open circles and black crosses represent ORPs obtained in the heating and cooling processes, respectively. In (d) and (e), green closed circles show ORPs observed in the heating process after keeping the samples at RT for more than one week. The sample cell thickness is about 20 μm and the temperature changing speed is 5°C/h.

and the carbon K-edge energy in this compound was 286 eV. In the following, actual RSoXS experiments were performed by irradiating samples with 285 eV (4.35 nm) incident beam. By fitting the x-ray profiles using the Lorentzian equation, the wavenumber of the periodicity was determined.

Experimental details of obtaining intensity autocorrelation functions by DLS were given in previous papers [35–37]. The samples were 25-μm-thick homeotropic cells. The vertically polarized argon ion laser (532 nm) was incident onto the sample cell at an angle of 18° to the substrate normal, and the perpendicularly polarized scattered light was observed by a photomultiplier from the substrate normal direction on the opposite side. The scattered intensity autocorrelation function

$$g^{(2)}(t) = \frac{\langle I(t')I(t'+t)\rangle}{\langle I(t')\rangle\langle I(t'+t)\rangle} \qquad (2)$$

was obtained by using a correlator (ALV-5000, ALV), which can cover a time range of 10^{-7} to 10 s [35]. Since the actual measurements were made at the early stage of the present investigations, the obtained results are rather preliminary in the sense that nominal sample concentrations were not monitored by observing ORPs and thus the concentrations were not sufficiently precisely recorded, and the superposition of homodyne and heterodyne signals was not carefully checked [36].

III. RESULTS AND DISCUSSION

A. ORP data and the existence of a single subphase with an exceptionally wide temperature stability range

In the bulk of MC881-MC452, Sandhya *et al.* [25,26] drew the T-r phase diagram by observing the Bragg reflection spectra from the macroscopic helical structure of the in-layer directors at various concentrations and temperatures. Actually, the existence of the subphase at a particular concentration can be confirmed rather easily by observing the dependence of ORP on temperature in the heating process as illustrated in Figs. 5(a), 5(b), and 5(c). It should be noted that the almost constant ORP of about 10∼15 deg observed from RT up to about 80°C indicates the stable existence of the subphase. Around 80°C the transition occurs between the subphase and the state with continuously changing q_T [25,26]. We can also see the emergence of the subphase even in the cooling process, but the transition temperature is always lower and its curve shape around the transition does not change much as the concentration increases. The relaxation to the subphase in the cooling process takes a very long time near the critical concentration r_c. In fact, as illustrated in Figs. 5(d) and 5(e), the ORP data looks not good because of the very long relaxation times at 58.50 and 59.00 wt.%. When we measure the ORP temperature variation in the heating process after keeping the sample cell at RT for a considerable time, however, it appears to show the subphase emergence from RT up to around 60 and 40°C for 58.50 and 59.00 wt.%, respectively. The long relaxation times for these concentrations disappear and the apparently ordinary ORP data of SmC^* is observed at 60.01 wt.% as seen in Fig. 5(f). Regarding the ORP temperature variation on the low concentration side, we have not yet performed any systematic study. The ORP data at 52.00 and 54.00 wt.% illustrated in Figs. 6(a) and 6(b), however, clearly indicate that the subphase boundary on the low concentration side is not a vertical straight line as depicted in Fig. 1 of Ref. [28]. The subphase that appears continuously from RT to above 80°C at 55.00 wt.% is divided into a high-temperature branch and a

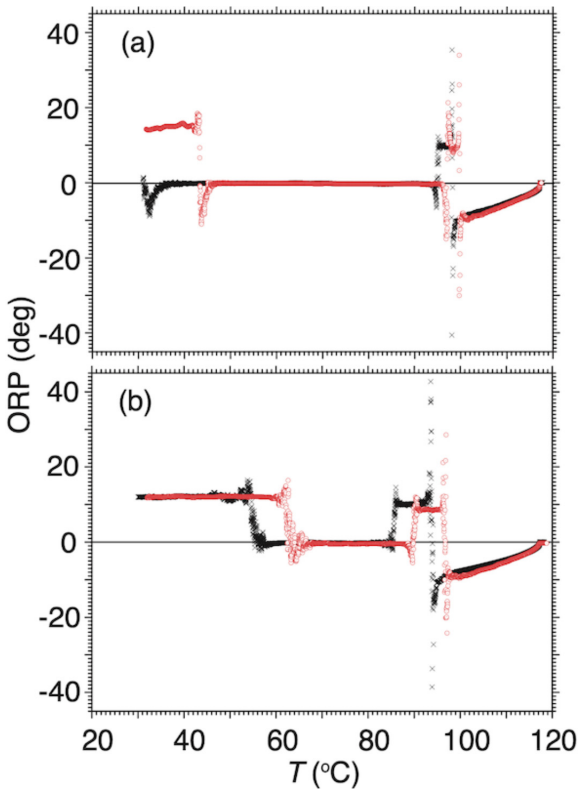

FIG. 6. ORP vs temperature in MC881 containing MC452 of (a) 52.00 and (b) 54.00 wt.%; red open circles and black crosses represent ORPs obtained in the heating and cooling processes, respectively. The sample cell thickness is about 20 μm and the temperature changing speed is 5°C/h.

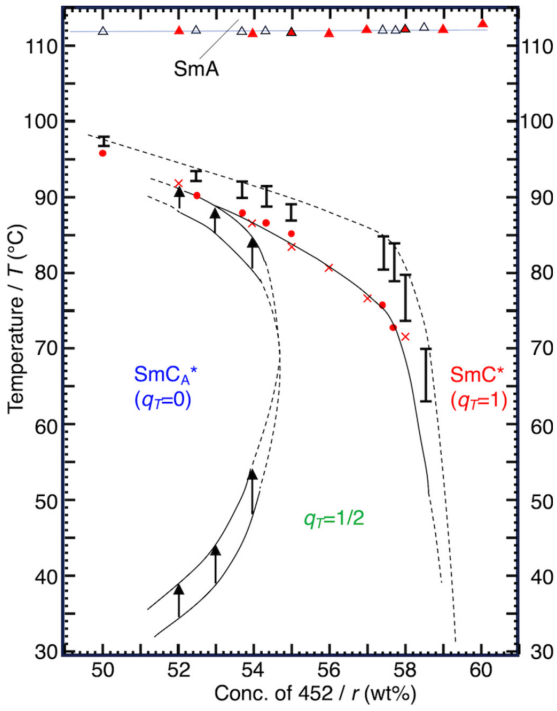

FIG. 7. Revised phase diagram of MC881-MC452 near critical concentration r_c. Three kinds of data Sandhya *et al.* used are: the transition temperatures to Sm*A* (open triangles), the temperature ranges where the full-pitch band gradually grows (bars with upper and lower limits), and the helical pitch diverging temperatures (full red circles). Two kinds of data added here are: the transition temperatures from the subphase to the state with continuously changing q_T (red crosses) and the temperature ranges where q_T changes continuously between 0 and 1/2 (black arrows) Red closed triangles is the transition temperature to Sm*A* are also added. Since the electric furnace is different from that used by Sandhya *et al.* Since the temperatures are slightly different overall, hence the over all temperatures have been shifted by about 4°C to match the phase transition temperature from Sm*C** to Sm*A*.

low-temperature branch (indicating black arrows in Fig. 7) by the emergence of SmC_A^* in between as seen at 52.00 to 54.00 wt.%; the Bragg reflection peak of nominally pure (*R*)-MC881 is about 400 nm and its ORP is negatively very small. The SmC_A^* stability temperature range gradually becomes wider as the concentration decreases from about 55.00 wt.%. It should be noted that the change between SmC_A^* and the subphase is not of the first order phase transition but occurs with the q_T number continuous varying. In fact, we can see the typical normal and abnormal dispersions in the ORP temperature variation between SmC_A^* and the subphase as in Figs. 6(a) and 6(b).

Here we tried to extend the phase diagram obtained by Sandhya *et al.* [25,26]. They used three kinds of the data: the transition temperatures to Sm*A*, the temperatures where the helical pitch diverges, and the temperature ranges where the full-pitch band grows gradually. We can add two kinds of data: one is the transition temperatures from the subphase to the state with continuously changing q_T that are a few degrees lower than the temperatures where ORP diverges, and the other is the temperature ranges where q_T changes continuously between 0 and 1/2. In this way, we depicted Fig. 7. The upward convexly curved solid line represents the upper boundary of the subphase, which starts to be blurred with increasing concentration at around 58.50 wt.%. Two lines curved concavely toward the left are the boundaries of the subphase and SmC_A^*; upward arrows represent the continuous change of q_T between 1/2 and 0. As the concentration approaches to 55.00 wt.%, the transition from the subphase to SmC_A^* would become difficult to occur smoothly because of the prolonged relaxation time.

Since the emergence of the corresponding subphase has not been confirmed in the bulk of MC881-MC815, we now move on to show its existence by observing the ORP temperature variation at several MC815 wt.% concentrations. After considerable experimental challenge, we obtained the rather systematic data as summarized in Fig. 8; difficulties encountered were the much longer relaxation time and the narrower concentration range of the stable subphase emergence in MC881-MC815 as compared with MC881-MC452. The almost constant ORP of about 10∼15 deg is observed from RT up to about 80°C as shown in Figs. 8(b), 8(c), and 8(d). Because of the much longer relaxation time, we need to reduce the temperature changing rate down to at least 2°C/h. At 31.63 and 31.75 wt.%, however, we could not obtain any meaningful ORP temperature variation as illustrated in Fig. 8(e) even at a temperature changing rate of 1°C/h. It

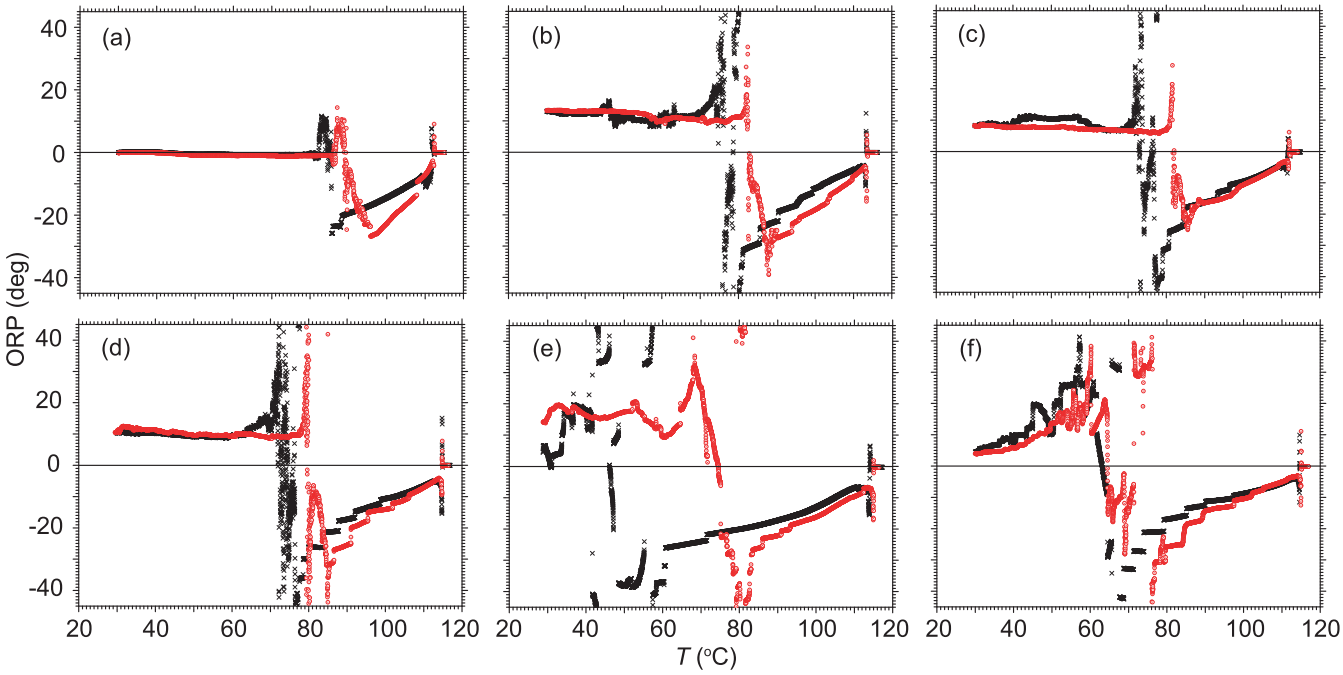

FIG. 8. ORP vs temperature in MC881 containing MC815 of (a) 30.64, (b) 30.87, (c) 31.11, (d) 31.36, (e) 31.63, and (f) 31.88 wt.%.; red open circles and black crosses represent ORPs obtained in the heating and cooling processes, respectively. The sample cell thickness is about 20 μm and the temperature changing speed is 2 or 1°C/h.

should be noted that, at 31.88 wt.%, the considerably long relaxation time disappears and the apparently ordinary ORP temperature variation indicating the emergence of SmC^* is observed as shown in Fig. 8(f). Although no detailed study has been performed as yet, the boundary on the high concentration side must be upward convexly curved. Regarding the phase boundary on the low concentration side, the ORP temperature variation data at 30.64 wt.% shown in Fig. 8(a) barely suggests that it is concavely curved toward the left; the subphase still exists at around 86°C and the continuous change from SmC_A^* with abnormal dispersion is observed. The phase diagram suggested at this stage was shown in Fig. 19 of Appendix. Anyway, both the boundaries on the low and high concentration sides seems to be not simple vertical straight lines not only in MC881-MC452 but also in MC881-MC815. As typically observed in Figs. 8(d) and 8(f), the negative ORPs in the high temperature region vary stepwise. This must be due to the surface anchoring that prevents the helical pitch from changing continuously.

B. Unit cell structures determined by RSoXS in the concentration and temperature range of the subphase

The rather systematic ORP vs temperature data clearly indicate the emergence of the subphase near the critical concentration r_c not only in MC881-MC452 but also in MC881-MC815 as described above in Sec. III A. Therefore we tried to determine their superlattice structures by x-ray scattering. The ordinary scattering factor is a scalar and hence is not sensitive to the clinicity. In resonant x-ray scattering (RXS), it becomes a tensor; by tuning the x-ray energy to the resonant energy of the specific atom, resonant satellite peaks show up in addition to the principal Bragg peaks. For a structure with n-layer periodicity, there appear satellite peaks at

$$\frac{Q_z}{Q_0} = l + m\left(\frac{1}{n} \pm \epsilon\right). \tag{3}$$

Here Q_z is the component of scattering vector along the smectic layer normal, $Q_0 = 2\pi/d$ with the layer spacing d, l and m are integers (±1, ±2, $\cdots$), and $\epsilon = 2\pi/p$ with the optical pitch p [8,14,38,39]. Several (ordinary and not TLAF) subphase superlattice structures have been clarified by RXS with LCs containing Br, Se, or S. These particular TLAF mixtures do not contain Br, Se, or S, so we need to use carbon K-edge (about 285 eV, 4.35 nm).

Figures 9(a) and 9(b) show resonant and off-resonant two-dimensional scattering images obtained from a membrane sandwich cell of MC881-MC815 at RT using incident x-ray with an energy of 285 eV (almost resonance condition) and of 270 eV (off-resonance condition), respectively. We can draw a typical resonant one-dimensional profile from the resonant two-dimensional scattering image, as illustrated in Fig. 9(c). The clear resonant peak observed at around $2\theta = 43.04$ deg, i.e., $Q_z = (4\pi/\lambda)\sin\theta = 1.06$ nm^{-1} corresponds to the periodicity of D=5.93 nm, which is nearly double the layer spacing d= 3.06 nm obtained by ordinary x-ray scattering, and hence indicates that the unit cell structure must be two-layer (AA) [8,14,38,39]. When the energy of incident x-ray is changed to 270 eV, this peak disappears completely as seen in Fig. 9(b). Unfortunately, however, some annoying background scattering signals are observed both in resonant and nonresonant conditions. These must be due to some poor monochromaticity of the soft x-ray source; we eliminate these

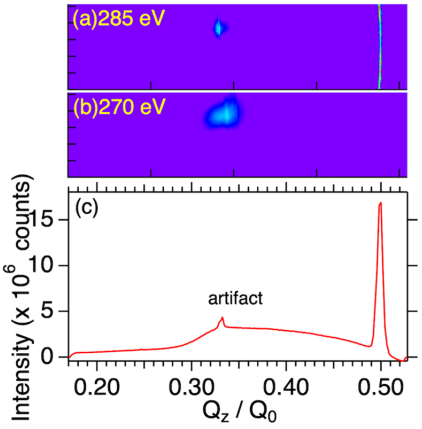

FIG. 9. Resonant and off-resonant soft x-ray scattering in a membrane sandwich cell of MC881 containing 31.11 wt.% MC815 at RT. (a) Resonant (285 eV) and (b) nonresonant (270 eV) two-dimensional images in measurement time of 180 s. Incident x-ray energy is indicated in the images. (c) One-dimensional intensity profile of the membrane sandwich cell depicted from panel (a).

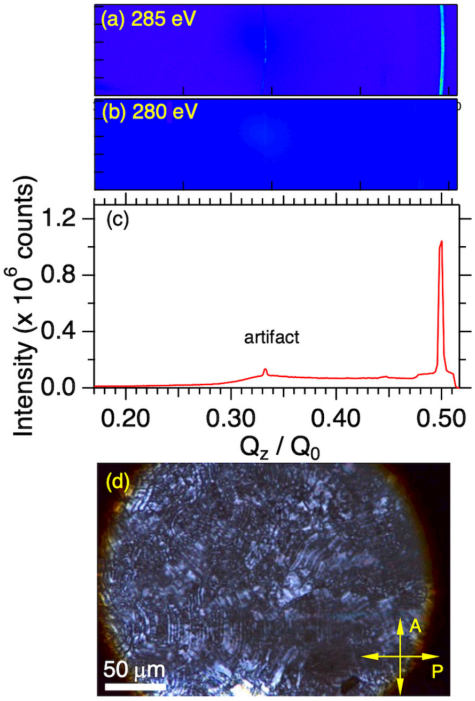

FIG. 10. Resonant and off-resonant soft x-ray scattering in a membrane sandwich cell of MC881 containing 55.70 wt.% MC452 at RT. (a) Resonant (285 eV) and (b) nonresonant (280 eV) two-dimensional images in measurement time of 180 s. (c) One-dimensional intensity profile of the membrane sandwich cell depicted from panel (a). (d) Optical microphotograph of the membrane sandwiched cell under the crossed polarizers.

by using several measures as below. Since the incident off-resonant energy (270 eV) is more than three times stronger than the incident resonant energy (285 eV), the off-resonant background scattering signal becomes stronger than the resonant ones as seen in Figs. 9(a) and 9(b).

The superlattice structure with the two-layer unit cell (*AA*) was also confirmed in a membrane sandwich cell of MC881-MC452. Figures 10(a) and 10(b) show resonant and off-resonant two-dimensional scattering images obtained in a membrane sandwich cell of MC881-MC452 at RT using incident x-ray with an energy of 285 eV (resonance condition) and of 280 eV (off-resonance condition), respectively. The one-dimensional profile obtained from Fig. 10(a) is also given in Fig. 10(c). Since we used several filters, the background scattering becomes weaker as compared in Fig. 9. The strong peak observed at $Q_z = 1.09\,\mathrm{nm}^{-1}$ in resonant scattering completely disappears in off-resonant scattering. This peak corresponds to a periodicity of $D = 5.76$ nm, which is nearly double the layer spacing $d = 2.98$ nm; hence the superlattice structure must have two-layer unit cell (*AA*) [8,14,38,39]. Polarized optical texture of the membrane sandwiched cell at RT is shown in Fig. 10(d). Optical axis seems to be parallel to the layer normal, suggesting the bilayer anticlinic structure.In this way it is well established that the subphase stabilized in an exceptionally wide temperature range has the superlattice structure with the two-layer unit cell (*AA*) and hence looks like SmC_A^* in the membrane sandwich cell of both mixtures of MC881-MC815 and MC881-MC452. However, previous investigations by Sandhya *et al.* and Feng *et al.* [24,25,28] confidently anticipated the $q_T = 1/2$ subphase with the four-layer unit cell (*FAFA*). The silicon nitride membrane interfaces must realize surface-stabilized SmC_A^*. Since the four-layer unit cell has the distortion angle δ [12,40,41] and the directors are not really parallel to the substrate plates, the sum of bulk and surface energies appear to prefer the much simpler two-layer unit cell of SmC_A^*. To directly clarify the inherent superlattice structure of the subphase, we used the TEM grid cell and obtained beautiful RSoXS results which unambiguously indicate that the subphase has the four-layer (*FAFA*) unit cell in the bulk. Figure 11 is the one-dimensional profiles obtained in the TEM grid cell of the same mixture MC881-MC452 at various temperatures using incident x-ray with the energy of 285 eV (resonance condition). Since there exist no membranes which absorb the incident 285 eV radiation, the background scattering signals become weak relatively. Compared to the membrane sandwich cell, the resonant scattering image is significantly different, with a scattering peak observed at a small angle, which is maintained up to around 90°C. The structural period obtained from the peak is $D = 12.09$ nm at RT. The splitting of the peak is due to the subphase macroscopic helical structure of about 2 μm [8,14,38,39].

Temperature dependence of the structural period is plotted from the scattering profile, as shown in Fig. 12(a). The structural period is almost four times the layer spacing, as shown in Fig. 12(b), which indicates a four-layer periodic structure. Furthermore, dielectric measurements of a homogeneous cell with a cell thickness of 6 μm showed antiferroelectric behavior from low temperatures upto around 85°C in Fig. 13, similar to that found by Feng *et al.* [28]. Therefore, it can be concluded that the smectic phase formed between RT and 85°C in the so-called bulk state has the superlattice structure (*FAFA*). The similar result to Fig. 11 was obtained from a TEM grid cell of MC881 containing with 31.11wt.% MC815 (see Fig. 20 of Appendix).

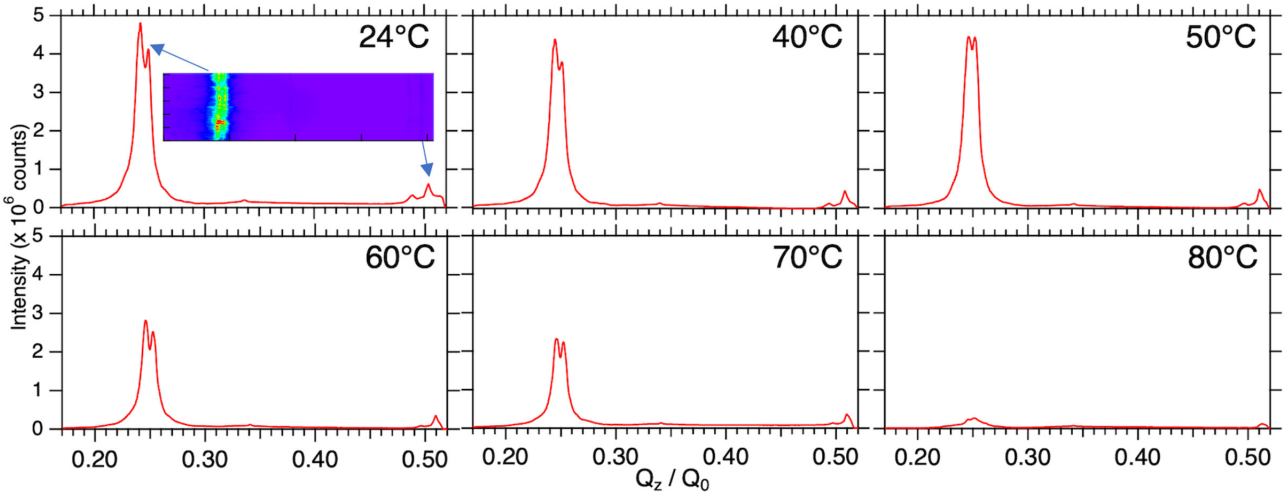

FIG. 11. One-dimensional intensity profile of the TEM grid cell in MC881 containing 55.70 wt.% MC452 at 24, 40, 50, 60, 70, and 80°C with the energy of 285 eV (resonance condition). At 24°C, the corresponding 2D image is displayed.

C. TLAF properties of the subphase and the responsible relaxation times

Now we are sure that, in thin enough cells of both TLAF mixtures at RT and around the middle of the subphase concentrations, the subphase transform into the two-layer (*AA*) unit cell structure, although the subphase itself has the four-layer (*FAFA*) superlattice structure in the bulk. Song *et al.* [42], without noticing the existence of the subphase, reported the TLAF response in 2-μm-thick homogeneous cell of MC881 containing 55 wt.% MC452 by observing apparent polarization as a function of the applied field. So we similarly try to check the TLAF response in MC881-MC815, and immediately notice that the thin (around 2.1-μm-thick) homogeneous cells are liable to become ferroelectric as illustrated in Fig. 14. The interfaces used are spin-coated by aligning polyimides RN1175 (Nissan Chemical Industries, Ltd.) and AL1254 (JSR Corporation), and a bare ITO substrate without polyimide coating; we also use some cells purchased from EHC Co., Ltd. (Japan). The interface-induced ferroelectricity always plays an important role, and we could not confirm the TLAF response even in the around 2 μm thick cell of MC881-MC452, either.

To get the full picture, we prepared a 300 nm∼5 μm wedge cell using bare ITO substrates and took micrographs as shown in Fig. 15. In the less than 1 μm region (upper left) we can see the multidomain texture similar to the one shown in Fig. 10(d), in which the optical axis is parallel to the layer normal, and hence the two-layer (*AA*) unit cell structure must be realized. Around 2 μm region (upper right and lower left) broken fan texture seems to be produced as in Fig. 14.

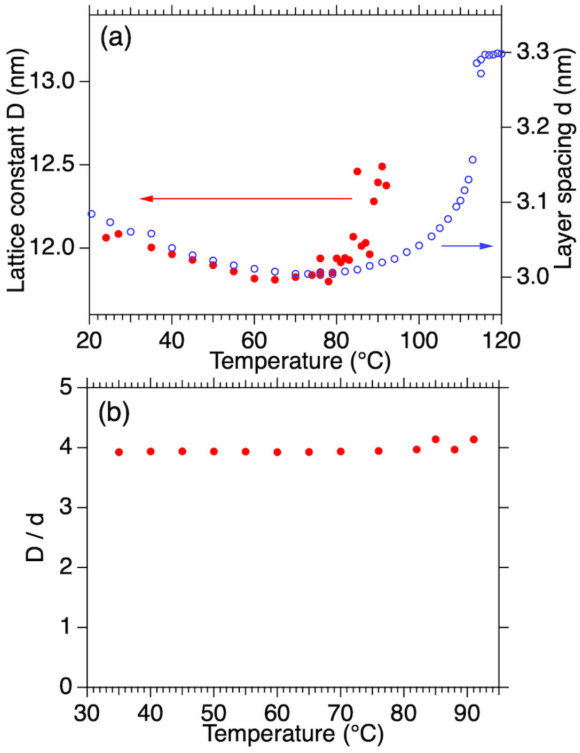

FIG. 12. (a) Temperature dependence of the periodicity D obtained from the TEM grid cell of MC881 containing 55.70 wt.% MC452 by RSoXS (red circle) and the layer spacing d by the conventional x-ray scattering (blue open circle). (b) Temperature dependence of D/d.

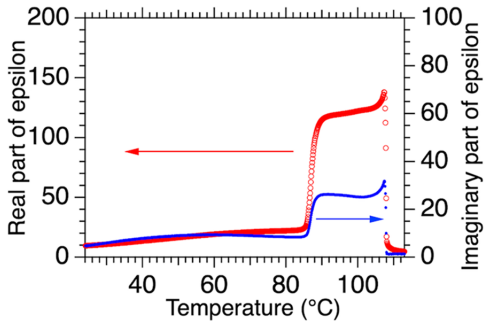

FIG. 13. Temperature dependence of the dielectric constant at 1 kHz of the 6-μm-thick homogeneous cell of MC881 containing 55.70 wt.% MC452. Red open circles and blue dots indicate the real and imaginary part of epsilon, respectively.

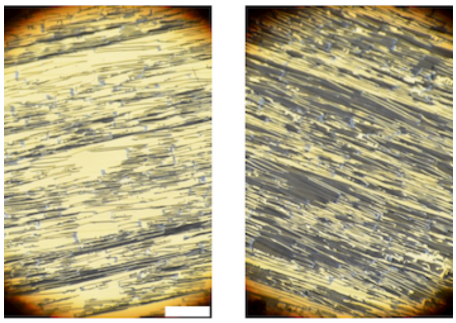

FIG. 14. Micrographs showing bistability due to the twisted states in MC881 containing 31.11 wt.% MC815. Note that the interfaces are more or less polar and force the spontaneous polarization in each layer to direct outwards or inwards [43–45]. White scale bar shows 100 μm

However, in the 5 μm region (lower right) texture in which the optical axis is parallel to the layer normal again is observed, suggesting that the four-layer (*FAFA*) superlattice structure seems to be realized. Not only in MC881-MC452 but also in MC881-MC815, actually, thick homogeneous cells show the TLAF response when we observe the apparent tilt angle vs applied field as illustrated in Fig. 16; the antiferroelectricity was confirmed by the detailed dielectric studies [28]. Although the RSoXS experiment indicates that the four-layer (*FAFA*) structure is fairly well established in the bulk, thermal fluctuations must cause occasional clinicity flip-flopping of a single layer, here and there, keeping its antiferroelectricity as a whole, and bring about the TLAF response. In fact, Shirota *et al.* [33] considered such clinicity flip-flopping of a single layer, when they studied the response to an applied electric field in thick homeotropic cells of MC881 containing 55.7 wt.% MC452; they suggested that the TLAF response must be observed in a homogeneous cell. To directly detect the clinicity flip-flopping of a single layer, we tried to observe intensity autocorrelation functions in DLS. We have not yet performed any systematic experiments, but some results are obtained in two MC881 mixtures containing 53.7 and 58.1 wt.% MC452 as well as in nominally pure MC881 and MC452 themselves. Typical intensity autocorrelation functions observed are illustrated in Fig. 17; there exist three components with fast, slow, and extremely slow relaxation times, τ_1, τ_2, and τ_3. Since τ_1 appears

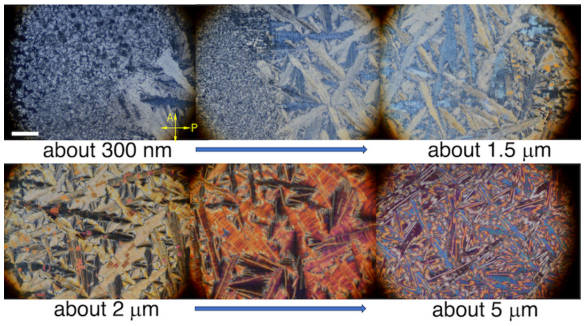

FIG. 15. Texture micrographs of a 300 nm∼5 μm wedge cell using bare ITO substrates in MC881 containing 31.11 wt.% MC815. White scale bar shows 100 μm.

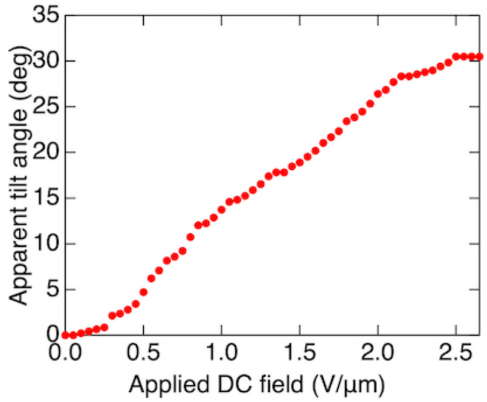

FIG. 16. Apparent tilt angle vs applied electric field observed at RT in a thick homogeneous cell of MC881 containing 31.11 wt.% MC815. The antiferroelectricity was directly confirmed by dielectric study; hence the q_T=1/2 subphase with the superlattice structure (*FAFA*) is realized at RT.

to be two orders of magnitude faster than τ_2, and furthermore τ_3 in time domain is longer than 1 s where measurements are less reliable, we try to fit the intensity autocorrelation function

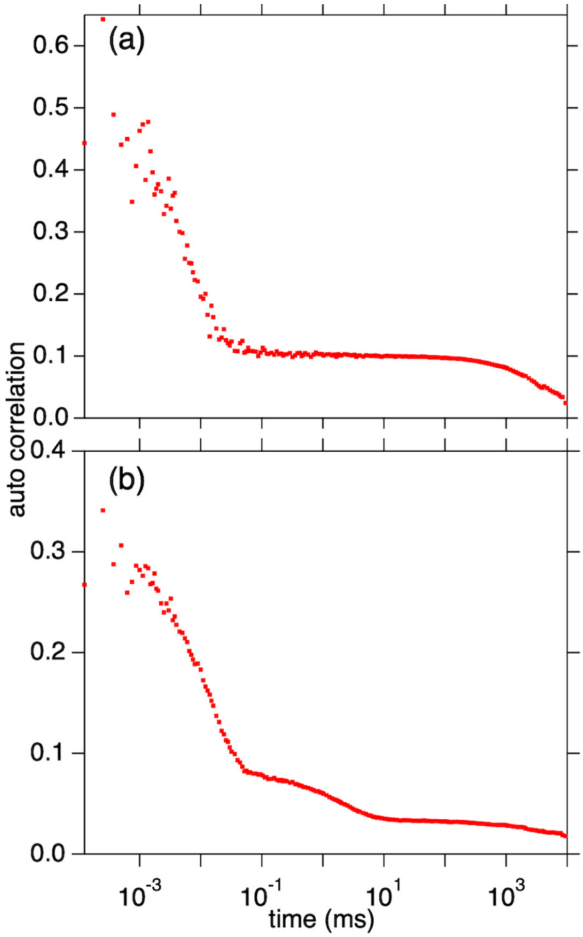

FIG. 17. Observed examples of intensity autocorrelation functions in MC881 containing 53.7 wt.% MC452 at (a) 65 and (b) 90°C.

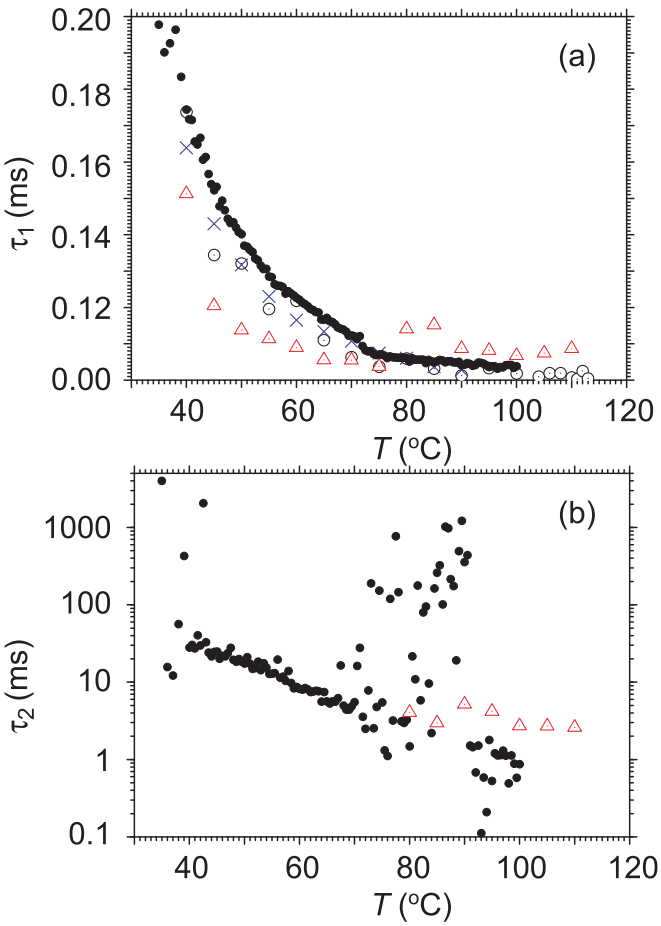

FIG. 18. Temperature dependence of (a) fast and (b) slow relaxation times, τ_1 and τ_2, in MC881 containing MC452 of (1) 0 wt.% (nominally pure MC881): black open circles, (2) 53.7 wt.%: red open triangles, (3) 58.1 wt.%: black closed circles, and (4) 100 wt.% (nominally pure MC452): black crosses.

to Eq. (4),

$$g^{(2)}(t) = a_1 \exp\left(-\frac{2t}{\tau_1}\right) + a_2 \exp\left(-\frac{2t}{\tau_2}\right) + b, \quad (4)$$

where we neglect dependence on τ_3.

In nominally pure MC881 and MC452, the autocorrelation function consists of a single component with the fast relaxation time τ_1 as shown in Fig. 18(a), which can be attributed to the phase mode or Goldstone mode in SmC_A^* and SmC^* [46–49]. In MC881 containing 58.1 wt.% MC452, however, there surely exists a component with the slow relaxation time τ_2 as shown in Fig. 18(b) in addition to the τ_1 component; we can see the τ_2 temperature variation rather nicely between 40 and 70°C where the subphase is expected to exist stably. Although we did not check the ORP temperature variation in this particular sample of MC881 containing 53.7 wt.% MC452, the previous results by Sandhya *et al.* indicate that the subphase does not appear around 80°C, but that q_T changes continuously from 0 (SmC_A^*) to 1 (SmC^*); in fact, the τ_2 component is observed above about 80°C. Miyachi *et al.* [50] observed the similar slow relaxation of the intensity autocorrelation function in the ferrielectric q_T=1/3 subphase with three-layer unit cell, and considered that it must originate from the dielectric constant fluctuations due to the clinicity flip-flopping of a single layer.

IV. CONCLUSIONS AND FUTURE ISSUES

We have studied binary mixtures developed as TLAF materials, MC881-MC452 and MC881-MC815, by utilizing ORP, RSoXS, and DLS. We first observed ORP systematically vs temperature in both mixture materials, and determined the concentration range of the subphase stable existence not only in MC881-MC452 but also in MC881-MC815. The temperature-concentration phase diagram was also depicted in MC881-MC452, which mostly confirm some of the previous results obtained by Sandhya *et al.* [25]. Two additional findings being made are: (1) The boundaries between SmC_A^* and the subphase are curved concavely toward the left, and the change between them is not an ordinary first order phase transition but occurs with q_T varying *continuously*. Each smectic layer appears to play an important role as a *mesoscopic* entity. (2) The boundaries between the subphase and SmC^* are upward convexly curved and the change between them occurs continuously as already evidenced by the gradual growth of the full pitch band [25]; the SmC^* boundary had not been definitely determined while the subphase boundary now is precisely determined since the ORP divergence is always observed. Although it would be difficult to understand the detailed shape of each curve on the diagram theoretically, the boundary curves are natural as SmC^* tends to emerge gradually below SmA with increasing ferroelectric ordering [25].

We carried out RSoXS experiments by using two samples, MC881 containing 55.70 wt.% MC452 and MC881 containing 31.11 wt.% MC815. The two-layer (AA) superlattice structure has been observed at RT for both mixtures in ordinary homogeneous cells of less than 1 μm thickness sandwiched between silicon nitride membranes; this must be the surface-stabilized structure of the subphase. After encountering some experimental difficulties we were able to obtain RSoXS signals from randomly oriented sample with a negligible solid-interfacial effect by using TEM grid cells. Thus, the ($FAFA$) four-layer superlattice structure, which has often been suggested by indirect experimental means [24,25,28], is now firmly established by RSoXS. Due to limited RSoXS machine time, only MC881 containing 31.11 wt.% MC815 and for MC881 containing 55.70 wt.% MC452 were studied, the concentrations of which are in around the middle of the subphase stable existing range. A future study will systematically measure both TLAF mixtures; in particular, it would be challenging to investigate the continuous change among SmC_A^*, the subphase, and SmC^* by RSoXS.

We have tried to confirm the TLAF response by making thin cells of 2.1 μm thickness, but such thin cells could not achieve antiferroelectricity due to ferroelectricity caused by interfacial effects. It seems necessary to reduce the concentration and to strengthen the antiferroelectricity. Needless to say, MC881 containing 55.70 wt.% MC452 shows antiferroelectricity in the bulk or thick cells. Furthermore, the thermal fluctuations play an important role, as already pointed out by Shirota *et al.* [33]. These fluctu-

ations can produce additional induced polarization without changing $q_T=1/2$ in an applied electric field. This additional polarization promotes the transition to SmC^* cooperatively with the ordinary induced polarization responsible for the pretransitional effect in homogeneous cells even when the helical structure exists; hence the TLAF response has really been observed.

Finally, the relaxation times responsible for the TLAF properties are studied within the constraints already discussed by measuring the intensity autocorrelation functions in DLS. In addition to the phase mode or Goldstone mode in SmC_A^* and SmC^* [46–49] with relaxation times faster than 100 μs, another mode with slower relaxation times of a few to several tens of ms are observed between 100°C and RT. A group of molecules in a layer appear to oscillate coherently, may flip-flop between R and S at least virtually, and this causes the slow mode of the intensity autocorrelation functions; here R and S refer to the clinicity orderings of smectic layers that produce polarization with a component parallel or antiparallel to the applied field [33]. Since the system under consideration is mesoscopic, there should exist a coherence (correlation) length in a smectic layer as Hayashi *et al.* [51] pointed out.

Thus a systematic study using all the three methods are effective in elucidating the full picture of this unique system. The most important conclusion of this study is that the subphase superlatice structure in the bulk state is well-ordered four-layer (*FAFA*), and its surface-stabilized state is two-layer (*AA*) ordered; it is completely different from the simplified model of the phase with TLAF based on the Langevin-type alignment, where the director tilting is uniform in a smectic layer but its azimuthal angle changes from layer to layer randomly [51,52]. The most intriguing finding here is, however, the characteristic mannar of the thermal fluctuations playing an important role in TLAF. When there exists an energy barrier between the ferroelectric and antiferroelectric energy minima as in the binary mixtures under consideration, the only possible way for the phase transition to occur was considered to be a nonhomogeneous process—i.e., solitary wave propagation—to overcome the energy barrier [42,53–55]. As we have already clearly shown that the actual situation is quite the opposite: A group of molecules in a single layer appear to flip-flop smoothly and the change among SmC_A^*, $q_T=1/2$, and SmC^* occurs with a continuously varying q_T; a single layer behaves independently as a mesoscopic entity. In the future, we would like to clarify the real cause of this peculiar and interesting behavior of these binary mixture materials near the region of critical concentration area.

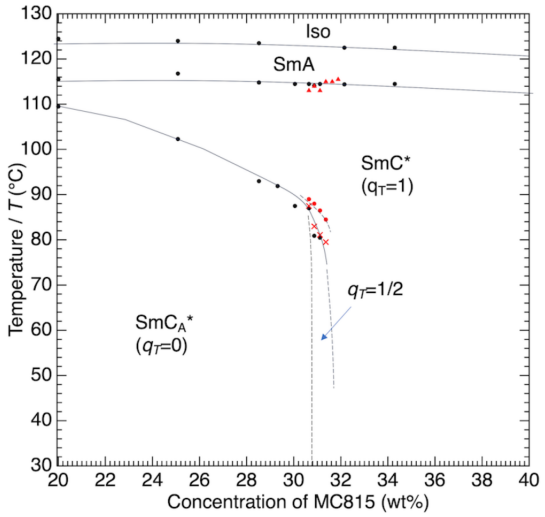

FIG. 19. Binary phase diagram of MC881-MC815 near critical concentrations. Red symbols (closed triangles, circles and crosses) are determined from Fig. 8, and black circles are the phase transition temperatures determined from the polarized microscope observations and dielectric measurements. It is suggested that red crosses correspond to the transition temperatures of the system from the lower temperatures phase (SmC_A^* or $q_T=1/2$) to the state with continuously changing q_T, and that red circles correspond to the transition temperatures to SmC*.

ACKNOWLEDGMENTS

MGC (Mitsubishi Gas Chemical Company, Inc.) is acknowledged for the gift of precious liquid crystal compounds, MC881, MC815, and MC452. The work in Dublin was funded by Research Ireland under US-Ireland collaborative program, Project No. SFI 21/US/3788 and the PI (J.K.V.) thanks the collaborative partners for discussion. The RSoXS measurements were performed at the BL3U of UVSOR Synchrotron Facility, IMS (IMS Programs No. 23IMS6819, No. 23IMS6621, and No. 24IMS6616) and with the approval of the Photon Factory Advisory Committee (Proposal No. 2025G118). Some funding was provided by JSPS Grant No. KAKENHI (21K2523). We thank Prof. Jun Yamamoto and Tomoyuki Morita for their help with the DLS measurements.

DATA AVAILABILITY

The data that support the findings of this article are openly available [1]; embargo periods may apply.

APPENDIX

1. Phase diagram of MC881-MC815 near critical concentrations

Figure 19 shows the binary phase diagram of MC881-MC815 near critical concentrations. This phase diagram is primally determined based on Fig. 8, with results from polarized microscope observations and dielectric measurements also taken into account as supporting results. For polarized microscope observations, 12-μm-thick homeotropic aligned cells were used while 16-μm-thick planar aligned cells were used for the dielectric measurements. At 30.64 wt.%, lower temperature phase was SmC_A^*, while it was $q_T=1/2$ at 30.87, 31.11, and 31.36 wt.%. At this stage, the transition temperatures from the subphase to the state with continuously changing q_T can only be suggested from the ORP results.

2. Resonant soft x-ray scattering result of the TEM grid cell in MC881 containing 31.11 wt.% MC815

Figure 20 is the one-dimensional RSoXS intensity profile obtained in the TEM grid cell of MC881 containing

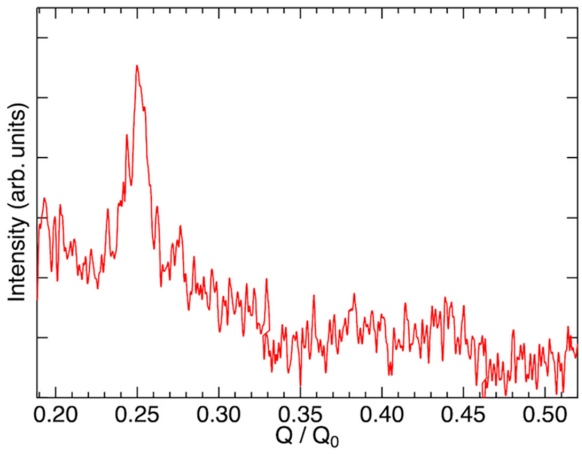

FIG. 20. One-dimensional RSoXS intensity profile obtained in the TEM grid cell of MC881 containing 31.11 wt.% MC815 at 40 °C. Incident x-ray energy is 285 eV (resonance condition), and Q_0 is the wavenumber of the single layer spacing of the same mixture.

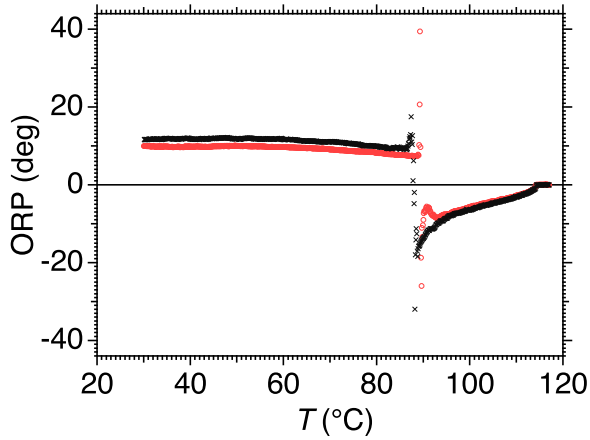

FIG. 21. Plot of the ORP data of MC815 containing 55.0 wt.% MC452. Red open circles and black crosses represent ORPs obtained in the heating and cooling cycles, respectively. The sample cell thickness is about 20 μm and the temperature scanning rate is 5 °C/h.

31.11 wt.% MC815 at 40 °C using incident x-ray with the energy of 285 eV (resonance condition). This experiment was performed at BL-7A of Photon Factory (Tsukuba). TEM grid cell was the same as shown in Figs. 2(b) and 2(c). Since the photon flux of 285 eV of this beam line is weaker than that of BL3U of UVSOR (Okazaki), the overall intensity is weak and the profile is noisy, but the RSoXS peak corresponding to the four layer periodicity is surely observed at around $Q/Q_0 = 0.25$.

3. ORP data of MC815 containing 55.0 wt.% MC452

Figure 21 shows temperature dependence of the optical rotatory power of MC815 containing 55.0 wt.% MC452. Measurement condition is the same as that in Fig. 5.

[1] R. B. Meyer, L. Liebert, L. Strzelecki, and P. Keller, Ferroelectric liquid crystals, J. Phys. Lett. (France) **36**, 69 (1975).

[2] R. B. Meyer, Ferroelectric liquid crystals: A review, Mol. Cryst. Liq. Cryst. **40**, 33 (1977).

[3] N. A. Clark and S. T. Lagerwall, Submicrosecond bistable electro-optic switching in liquid crystals, Appl. Phys. Lett. **36**, 899 (1980).

[4] A. D. L. Chandani, E. Gorecka, Y. Ouchi, H. Takezoe, and A. Fukuda, Antiferroelectric chiral smectic phases responsible for the tristable switching in MHPOBC, Jpn. J. Appl. Phys. **28**, L1265 (1989).

[5] Here the micrometer-sized helical structures due to the weak chiral interactions are not taken into consideration so that the biaxial subphases are commensurate.

[6] H. Takezoe, E. Gorecka, and M. Cepic, Antiferroelectric liquid crystals: Interplay of simplicity and complexity, Rev. Mod. Phys. **82**, 897 (2010).

[7] P. V. Dolganov and E. I. Kats, Landau theory description of polar smectic structures, Liq. Cryst. Rev. **1**, 127 (2013).

[8] C. C. Huang, S. Wang, L. Pan, Z. Q. Liu, B. K. McCoy, Y. Sasaki, K. Ema, P. Barois, and R. Pindak, Liquid crystal mesophases beyond commensulate four periodicity, Liq. Cryst. Rev. **3**, 58 (2015).

[9] M. A. Osipov and A. Fukuda, Molecular model for the anticlinic smectic-C_A phase, Phys. Rev. E **62**, 3724 (2000).

[10] M. A. Osipov and A. Fukuda, Synclinic and anticlinic ordering in frustrated smectics, Mol. Cryst. Liq. Cryst. **402**, 9 (2003).

[11] M. A. Osipov, A. Fukuda, and H. Hakoi, Synclinic and anticlinic ordering in frustrated smectics, Mol. Cryst. Liq. Cryst. **402**, 9 (2003).

[12] A. V. Emelyanenko and M. A. Osipov, Theoretical model for the discrete flexoelectric effect and a description for the sequence of intermediate smectic phases with increasing periodicity, Phys. Rev. E **68**, 051703 (2003).

[13] K. L. Sandhya, J. K. Vij, A. Fukuda, and A. V. Emelyanenko, Degeneracy lifting near the frustration points due to long-range interlayer interaction forces and resulting varieties of polar chiral tilted smectic phases, Liq. Cryst. **36**, 1101 (2009).

[14] Z. Feng, A. D. L. Chandani Perera, A. Fukuda, J. K. Vij, K. Ishikawa, A. Iida, and Y. Takanishi, Definite existence of subphases with eight- and ten-layer unit cells as studied by complementary methods, electric-field-induced birefringence and microbeam resonant x-ray scattering, Phys. Rev. E **96**, 012701 (2017).

[15] Y. Takanishi, A. Iida, N. Yadav, A. D. L. Chandani Perera, A. Fukuda, M. A. Osipov, and J. K. Vij, Unexpected electric-field-induced antiferroelectric liquid crystal phase in SmC^*_α temperature range and the discrete flexoelectric effect, Phys. Rev. E **100**, 010701(R) (2019).

[16] A. Fukuda, J. K. Vij, and Y. Takanishi, Variety of subphase emerging sequences, the frustration of three main phases, SmC^*_A, SmC^*, and SmA, and the long-range interlayer interactions, Phys. Rev. E **104**, 014705 (2021).

[17] J.-K. Song, A. D. L. Chandani, A. Fukuda, J. K. Vij, I. Kobayashi, and A. V. Emelyanenko, Temperature-induced sign reversal of biaxiality observed by conoscopy in some ferroelectric Sm-C^* liquid crystals, Phys. Rev. E **76**, 011709 (2007).

[18] J. Prost and R. Bruinsma, Fluctuation forces and the Devil's staircase of ferro/antiferroelectric smectic C*s, Ferroelectrics **148**, 25 (1993).

[19] R. Bruinsma and J. Prost, Fluctuation forces and the Devil's staircase of ferroelectric smectic C*s, J. Phys. (France) **4**, 1209 (1994).

[20] C. Tanaka, T. Fujiyama, T. Maruyama, and S. Nishiyama, Antiferroelectric liquid crystal with a novel hysteresis loop [in Japanese], Abstr. Jpn. Liq. Cryst. Conf., 250 (1995).

[21] Y. Yoshioka, M. Johno, T. Yui, and T. Matsumoto, Liquid crystal composition, Euro. Pat. Appl., EP1039329 (2000).

[22] T. Matsumoto, A. Fukuda, M. Johno, Y. Motoyama, T. Yui, S.-S. Seomun, and M. Yamashita, A novel property caused by frustration between ferroelectricity and antiferroelectricity and its application to liquid crystal displays—Frustoelectricity and V-shaped switching, J. Mater. Chem. **9**, 2051 (1999).

[23] A. Fukuda, Y. Takanishi, T. Isozaki, K. Ishikawa, and H. Takezoe, Feature article: Antiferroelectric chiral smectic liquid crystals, J. Mater. Chem. **4**, 997 (1994).

[24] K. L. Sandhya, A. D. L. Chandani-Perera, A. Fukuda, J. K. Vij, and K. Ishikawa, Antiferroelectric and ferroelectric orderings in frustrated chiral tilted smectics and a continuous change from anticlinic SmC_A^* to synclinic SmC^*, Europhys. Lett. **90**, 56005 (2010).

[25] K. L. Sandhya, A. D. L. Chandani, A. Fukuda, J. K. Vij, A. V. Emelyanenko, and K. Ishikawa, Degeneracy lifting due to thermal fluctuations around the frustration point between anticlinic antiferroelectric SmC_A^* and synclinic ferroelectric SmC^*, Phys. Rev. E **87**, 012502 (2013).

[26] A. Fukuda, What are thresholdless antiferroelectric (TLAF) LCs?—Disordered SmC*-like phase with q_T=1/2 in a wide temperature range, Mol. Cryst. Liq. Cryst. **610**, 1 (2015).

[27] T. Matsumoto, Development of the liquid crystal materials showing V-shape switching, in *Proceedings of the 8th International Conference of Ferroelectric Liquid Crystals* (2001).

[28] Z. Feng, V. Swaminathan, V. P. Panov, A. Fukuda, K. Ishikawa, and J. K. Vij, Dielectric study of a subphase stabilized in an exceptionally wide temperature range by a delicate balance of interlayer interactions and thermal fluctuations, Phys. Rev. E **102**, 012703 (2020).

[29] C. Zhu, M. R. Tuchband, A. Young, M. Shuai, A. Scarbrough, D. M. Walba, J. E. Maclennan, C. Wang, A. Hexemer, and N. A. Clark, Resonant carbon K-edge soft x-ray scattering from lattice-free heliconical molecular ordering: Soft dilative elasticity of the twist-bend liquid crystal phase, Phys. Rev. Lett. **116**, 147803 (2016).

[30] Y. Takanishi, F. Araoka, and H. Iwayama, The effect of the structure of helical nanofilament of the B4 phase of bent-core liquid crystals on the nano-phase separation mixed with rod-like cholesteric liquid crystal mixture, RSC Adv. **12**, 29346 (2022).

[31] J.-J. Lee, S. Kim, H. Nishikwa, Y. Takanishi, H. Iwayama, C. Kim, S.-W. Choi, and F. Araoka, Chiroptical performances in self-assembled hierarchical nanosegregated chiral intermediate phases composed of two different achiral bent-core molecules, Int. J. Mol. Sci. **23**, 14629 (2022).

[32] A. D. L. Chandani, N. M. Shtykov, V. P. Panov, A. V. Emelyanenko, A. Fukuda, and J. K. Vij, Discrete flexoelectric polarizations and biaxial subphases with periodicities other than three and four layers in chiral smectic liquid crystals frustrated between ferroelectricity and antiferroelectricity, Phys. Rev. E **72**, 041705 (2005).

[33] K. Shirota, A. Fukuda, N. Yadav, V. P. Panov, J. K. Vij, Y. Yamagata, and K. Ishikawa, Response to an applied electric field in an antiferroelectric 1/2 subphase: The role of thermal fluctuations, Phys. Rev. E **107**, 064701 (2021).

[34] Z. Feng and K. Ishikawa, Development of simultaneous measurement system of birefringence, optical rotational power, and transmission spectra for chiral liquid crystal phases, Jpn. J. Appl. Phys. **55**, 050301 (2016).

[35] Y. Yamazaki, Y. Takanishi, and J. Yamamoto, Dynamic heterogeneity of a nanostructure in the hyper-swallen B4 phase of achiral bent-core molecules diluted with rod-like liquid crystals, Europhys. Lett. **88**, 56004 (2009).

[36] R. Akiyama, K. Tomida, Y. Endo, H. Murooka, A. Fukuda, and E. Kuze, Homodyne and heterodyne problems in measuring spectral width of polarized Rayleigh line scattered by nematic liquid crystals, Jpn. J. Appl. Phys. **22**, L769 (1983).

[37] G.-P. Chen, H. Takezoe, and A. Fukuda, Determination of K_i (i=1-3) and μ_j (j=2-6) in 5CB by observing the angular dependence of Rayleigh line spectral widths, Liq. Cryst. **5**, 341 (1989).

[38] P. Mach, R. Pindak, A.-M. Levelut, P. Barois, H. T. Nguyen, H. Baltes, M. Hird, K. Toyne, A. Seed, J. W. Goodby, C. C. Huang, and L. Furenlid, Structures of chiral smectic-C mesophases revealed by polarization-analyzed resonant x-ray acattering, Phys. Rev. E **60**, 6793 (1999).

[39] A.-M. Levelut and B. Pansu, Tensorial x-ray structure factor in smectic liquid crystals, Phys. Rev. E **60**, 6803 (1999).

[40] I. Musevic and M. Skarabot, Optical rotation and structure of ferrielectric smectic phases, Phys. Rev. E **64**, 051706 (2001).

[41] M. Cepic and H. Gleeson, Phases with short periods, in *Handbook of Liquid Crystals*, 2nd ed., edited by J. W. Goodby, P. J. Collings, T. Kato, C. Tschierske, H. F. Gleeson, and P. Raynes (Willey-VCH, Weinheim, 2014), Vol. 4, p. 417.

[42] J. K. Song, A. Fukuda, and J. K. Vij, Gradual phase transition between the smectic-C^* and smectic-C_A^* phases and the thresholdless antiferroelctricity, Phys. Rev. E **78**, 041702 (2008).

[43] M. A. Handschy, N. A. Clark, and S. T. Lagerwall, Field-induced first-order orientation transitions in ferroelectric liquid crystals, Phys. Rev. Lett. **51**, 471 (1983).

[44] M. Glogarova and J. Pavel, The structure of chiral Sm C* liquid crystals in planar samples and its change in an electric field, J. Phys. (France) **45**, 143 (1984).

[45] N. Hiji, Y. Ouchi, H. Takezoe, and A. Fukuda, Structure of twisted states in ferroelectric liquid crystals studied by microspectrophotometry and numerical calculations, Jpn. J. Appl. Phys. **27**, 8 (1988).

[46] I. Musevic, R. Blinc, B. Zeks, C. Filipic, M. Copic, A. Seppen, P. Wyder, and A. Levanyuk, Observation of phason dispersion in a ferroelectric liquid crystal by light scattering, Phys. Rev. Lett. **60**, 1530 (1988).

[47] I. Drevensek, I. Musevic, and M. Copic, Dispersion of the Sm-C order-parameter fluctuations in the Sm-A and Sm-C phases

of 4-(2'-methylbutyl) phenyl 4'-n-octylbiphenyl-4-carboxylate, Phys. Rev. A **41**, 923 (1990).

[48] H. Sun, H. Orihara, and Y. Ishibashi, Observation of the phase mode in an antiferroelectric liquid crystal by photon correlation technique, J. Phys. Soc. Jpn. **60**, 4175 (1991).

[49] H. Sun, H. Orihara, and Y. Ishibashi, Relaxation mode and visco-elastic properties in an antiferroelectric liquid crysral (R)-MHPOBC observed by photon-correlation spectroscopy, J. Phys. Soc. Jpn. **62**, 2066 (1993).

[50] K. Miyachi, M. Kabe, K. Ishikawa, H. Takezoe, and A. Fukuda, Fluctuation in the ferrielectric smectic-C* phase as observed by laser beam diffraction and photon correlation spectroscopy, Ferroelectrics **147**, 147 (1993).

[51] N. Hayashi, T. Kato, T. Aoki, T. Ando, A. Fukuda, and S.-S. Seomun, Probable Langevin-like director reorientation in an interface-induced disordered SmC^*-like state of liquid crystals characterized by frustration between ferro- and antiferroelectricity, Phys. Rev. Lett. **87**, 015701 (2001).

[52] S. Inui, N. Iimura, T. Suzuki, H. Iwase, K. Miyachi, Y. Takanishi, and A. Fukuda, Thresholdless antiferroelectricity in liquid crystals and its application to display, J. Mater. Chem. **6**, 671 (1996).

[53] J.-F. Li, X.-Y. Wang, E. Kangas, P. L. Taylor, C. Rosenblatt, Y. I. Suzuki, and P. E. Cladis, Reversible propagating fingers in an antiferroelectfic liquid crystal, Phys. Rev. B **52**, R13075 (1995).

[54] J.-K. Song, A. Fukuda, and J. K. Vij, Solitary wave propagation in antiferroelectric liquid crystal cells and the quadrupolar term in the interlayer interaction, Phys. Rev. E **76**, 011708 (2007).

[55] J.-K. Song, A. Fukuda, and J. K. Vij, Dynamic mechanism of the ferroelectric to antiferroelectric phase transition in chiral smectic liquid crystals, Phys. Rev. Lett. **101**, 097801 (2008).